UC San Diego

UC San Diego Previously Published Works

Title

Electrochemical reaction and surface chemistry for performance enhancement of a Si composite anode using a bis(fluorosulfonyl)imide-based ionic liquid

Permalink

https://escholarship.org/uc/item/7106r550

Journal

Journal of Materials Chemistry A, 4(39)

ISSN

2050-7488

Authors

Shobukawa, H
Shin, J
Alvarado, J
et al.

Publication Date

2016

DOI

10.1039/c6ta06447g

Peer reviewed

eScholarship.org Powered by the California Digital Library
University of California

Journal of Materials Chemistry A

PAPER

View Article Online
View Journal | View Issue

Published on 30 August 2016. Downloaded by University of California - San Diego on 10/15/2019 6:23:28 PM.

Cite this: J. Mater. Chem. A, 2016, 4, 15117

Electrochemical reaction and surface chemistry for performance enhancement of a Si composite anode using a bis(fluorosulfonyl)imide-based ionic liquid†

Hitoshi Shobukawa,[ac] JaeWook Shin,[a] Judith Alvarado,[ab] Cyrus S. Rustomji[a] and Ying Shirley Meng*[a]

Received 29th July 2016
Accepted 30th August 2016

DOI: 10.1039/c6ta06447g

www.rsc.org/MaterialsA

An ionic liquid (IL) electrolyte with 1-ethyl-3-methylimidazolium bis(fluorosulfonyl)imide (EMIFSI) is applied to a silicon (Si) composite anode for Lithium-ion batteries (LIB). Si is one of the most promising anode materials for LIBs and fluoroethylene carbonate (FEC) has been widely used as an electrolyte additive with Si anodes to enhance electrochemical performance. However, the effect of FEC only lasts for a limited number of cycles. To overcome this issue, a bis(fluorosulfonyl)imide (FSI)-based IL is studied as a potential electrolyte candidate for a Si composite anode. Its effects on the electrochemical performance and the corresponding solid electrolyte interphase (SEI) formation on the Si composite anode are not well understood. This work addresses the correlation between the electrochemical performance and SEI formation to probe the surface chemistry on the Si composite anode. We find that the FSI-based electrolyte provides a stable and reversible capacity in long term cycling tests. This electrolyte has excellent rate capability compared to that of carbonate-based electrolytes. The decomposition products of these electrolytes on Si anodes are investigated by X-ray photoelectron spectroscopy. These results show that the chemical composition on the surface of the Si anode is largely different when using the FSI-based electrolyte than it is when using carbonate type electrolytes. The decomposition products of the IL lead to a large number of inorganic species such as LiOH and Li_2O, which yield superior rate capability for the IL electrolyte. The FSI-based IL offers promising applicability for a practical Si composite anode.

Introduction

Rechargeable batteries are essential to enable portable consumer electronics and are vital to the electric vehicles market. Lithium ion batteries (LIBs) have become the most important rechargeable batteries for numerous applications due to their high specific energy density.[1,2] So far, the specific energy density of LIBs has been increased mainly by improving the battery fabrication or by optimizing the electrode design, however, achieving higher energy density is still challenging.[3–6] Silicon (Si) is one of the most attractive anode materials because of its high theoretical capacity of 3579 mA h g^{-1} (about 10 times larger than that of graphite), earth-abundance, and environmental benignity.[7] Si is widely used in the semiconductor industry and solar industry whose techniques and expertise may help mass manufacturing.[8–13] However, there are two challenges to overcome in order to commercialize Si anodes for LIBs. First is the physical challenge: Si is mechanically pulverized during the charge and discharge process. This is because the particle volume continues to expand and contract from the electrochemical alloying/dealloying reaction between Li and Si.[14–16] Second is the chemical challenge: electrolyte degradation during electrochemical cycling forms a solid-electrolyte interphase (SEI) on the Si surface. Repeated expansion and contraction cause a severe volume change at the interface which forms a thick insulating SEI.[17,18] An unstable SEI lowers the coulombic efficiency (C.E.) and deteriorates the capacity retention during charge and discharge.

The electrolyte is one of the key factors determining the battery performance; the electrolyte influences both the electrochemical capacity and voltage profiles, as well as the SEI formation. Vinylene carbonate (VC) and fluoroethylene carbonate (FEC) are commonly used as electrolyte additives. They are known to improve the C.E. and capacity retention by

[a]Department of NanoEngineering, University of California San Diego, 9500 Gilman Drive, La Jolla, CA 92093, USA. E-mail: shirleymeng@ucsd.edu

[b]Materials Science and Engineering Program, University of California San Diego, La Jolla, CA, USA

[c]Corporate Research & Development Center, Asahi Kasei, 1-105 Kanda Jinbocho, Chiyoda-ku, Tokyo 101-8101, Japan

† Electronic supplementary information (ESI) available. See DOI: 10.1039/c6ta06447g

Published on 30 August 2016. Downloaded by University of California - San Diego on 10/15/2019 6:23:28 PM.

forming a stable SEI not only on Si anodes, but also on graphite anodes.[19] Nevertheless, Schroder and coworkers have suggested that the FEC diminishes through cycling, leaving the majority of solvent components reduced on the Si anode and creating a less ideal SEI.[20]

Room temperature ionic liquids (ILs) have attracted much attention as alternative electrolytes. Currently, the decomposition products of ILs are not well understood despite their enticing solvent characteristics: high ionic conductivity, low volatility, negligible vapor pressure, and thermal stability.[21,22] Generally, the electrolytes used in LIBs are carbonate-based solvents, and $LiPF_6$ is used as the salt. It has been reported that the decomposition of these electrolytes leads to gas evolution in the cells during the battery performance raising safety concerns.[23] Therefore, IL electrolytes have several advantages over carbonate-based electrolytes, making them better candidates for the development of LIBs with a longer cycle life and better safety.

Recently, studies by Lee and Ishikawa reported the use of IL electrolytes, based on bis(fluorosulfonyl)imide (FSI) for LIBs.[24,25] The FSI-based IL is stable in the cathodic and anodic voltage windows (for graphite and Si), exhibiting a good cycling performance without any extra solvents or additives. However, there are only a few reports describing the electrochemical performance and interfacial reaction between an IL and a Si composite anode. In this work, we especially focus on 1-ethyl-3-methylimidazolium bis(fluorosulfonyl)imide (EMIFSI) as a promising electrolyte for a Si composite anode. We compare the electrochemical performance of the Si composite anode in lithium bis(fluoromethanesulfonyl) imide (LiFSI)/EMIFSI to that in conventional carbonate type electrolytes: $LiPF_6$/ethylene carbonate (EC)/diethyl carbonate (DEC), and $LiPF_6$/EC/DEC/FEC. Moreover, we investigate the decomposition products of the IL to determine their effects on electrochemical performance. This study suggests that the combination of a Si composite anode and an IL electrolyte has the potential to achieve high electrochemical performance correlated with low interfacial resistance and stable capacity. Additionally, we find that compared to the carbonate-based electrolytes, the LiFSI/EMIFSI electrolyte enhances the rate capability of the Si anode. Using XPS analysis, we discover that the SEI derived from the IL consists of more inorganic species (such as LiOH, Li_2O, and LiF) than that derived from carbonate-based electrolytes. We propose that these species are responsible for the high rate capability of the LiFSI/EMIFSI cycled Si anode.

Experimental methods

Electrode fabrication

Si nanoparticles (average particle size: 50 nm, Alfa Aesar) were used as the active material of the electrode. The Si composite anode was fabricated as follows: 50 wt% nano-Si powder, 25 wt% Ketjenblack (EC-600JD, Akzo Nobel), and 25 wt% sodium carboxymethyl cellulose (CMC-Na, DS = 0.9, M_w = 250 000, Sigma-Aldrich) were mixed in water. The obtained slurry was coated on a copper foil by using a doctor blade with 125 μm gap and dried at 100 °C for 20 hours under a vacuum to completely remove any water traces on the surface. The electrode sheet was cut into a disk and used for the battery tests. The mass of the Si active material on the electrode was 0.45 mg cm^{-2}, which is equivalent to 1.6 mA h cm^{-2}. This electrode was used to assemble a 2032 coin cell using a polymer separator (C480, Celgard Inc., USA). The carbonate electrolytes were solutions of 1 M $LiPF_6$ dissolved in EC/DEC 1 : 1 wt% (Selectilyte LP40, Battery grade, BASF) and EC/DEC/FEC 45 : 45 : 10 wt% (Selectilyte A6, Battery grade, BASF). The IL electrolyte was prepared by dissolving LiFSI (Nippon Shokubai Co., Ltd.) in EMIFSI (Solvionic Co., Ltd.) at a concentration of 0.6 mol kg^{-1} and was used without further purification. This electrolyte is referred to as LiFSI/EMIFSI. A small excess of electrolyte was added to each coin cell to prevent the electrolyte from drying out in the cell. A glass fiber GF/F (Whatman) filter was used as the separator for the IL electrolyte. The water content of each electrolyte was determined to be less than 20 ppm by Karl Fischer titration. Battery-grade lithium metal was chosen as the counter electrode. Coin cells were assembled in a glovebox purged with high purity Ar gas and maintained with water vapor levels at or below 5 ppm.

Electrochemical tests

After the coin cells were assembled, electrochemical performance tests were performed using an Arbin battery cycler in galvanostatic mode, limiting the charge and discharge potentials to 1.0 V and 0.05 V *vs.* the Li counter electrode (note that "charge" here refers to lithium intercalation into the Si anode or lithiation). The open circuit voltage of the coin cells was monitored for 10 hours and then the cells were charged and discharged with a current density of 70 μA cm^{-2}, which approximately corresponds to a C-rate of C/12. The percent capacity retention was calculated with respect to the first discharge capacity. Cyclic voltammetry (CV) measurements were carried out at a sweep rate of 1 mV s^{-1}. Additional electrochemical impedance spectroscopy (EIS) measurements were conducted over the frequency range scanned from 1 MHz to 0.01 Hz in the fully lithiated states. The impedance was collected by using a Solartron 1287 electrochemical interface after the first cycle and the 50th cycle. ZView software was used to fit the collected EIS spectra to the equivalent circuit. All electrochemical measurements were carried out at 20 °C.

Scanning electron microscopy (SEM)

After the electrochemical cycling, the coin cells were disassembled and the Si anodes were rinsed with acetonitrile to remove the residual electrolyte and dried in an Ar-filled glovebox. The surface and cross sectional images of the Si anode were collected with a field emission environmental SEM (Philips XL30).

X-ray photoelectron spectroscopy (XPS)

The chemical compositions of Si anode surfaces were analyzed after 100 electrochemical cycles, using XPS. All cycled samples were measured in the lithiated state. After the coin cells were disassembled in an Ar-filled glovebox, Si anodes were rinsed with acetonitrile and transferred in a vacuum tube to the

 This journal is © The Royal Society of Chemistry 2016

Published on 30 August 2016. Downloaded by University of California - San Diego on 10/15/2019 6:23:28 PM.

glovebox connected to the XPS chamber; samples were not exposed to the air. The washed electrodes were transferred to the ultrahigh-vacuum environment using a reduced oxidation (ROx) interface designed for transferring air-sensitive samples. The ROx incorporates methods and figures of merit to determine whether or not the samples have been exposed to additional traces of oxygen and water, other than in the glovebox environment, including during pump-down. The methods and components of the ROx are described in detail in a publication by Schroder and coworkers.[26] XPS was performed using a Kratos Ultra DLD XPS. Analysis followed similar methods to those employed in previous work.[20] All XPS measurements were collected with a 300 μm × 700 μm spot size without using a charge neutralizer during acquisition. Survey scans were collected with a 1.0 eV step size, and were followed by high-resolution scans with a step size of 0.05 eV for carbon 1s, oxygen 1s, lithium 1s, fluorine 1s, nitrogen 1s, and phosphorus 2p regions.

Fits of the XPS spectra were performed with CasaXPS software (version 2.3.15, Casa Software Ltd.) to estimate the atomic compositions and chemical species comprising the SEI. All fitting followed a self-consistent method similar to that described in our previous publications.[26,27] All SEI species were assumed to be electronically insulating and therefore were fitted with linear backgrounds and with Voigt functions composed of 15% Lorentzian and 85% Gaussian functions.[16,28–32] Initial peak fits were made of the spectra using the Levenberg–Marquardt least-squares algorithm, and atoms with the same functionality were assumed to be stoichiometric. The resulting spectra were then refitted and all spectra were shifted relative to the binding energy of the carbon 1s sp^3 (assigned to 284.8 eV) to compensate for any offset during the measurement.

Ionic conductivity measurement

Electrolytic conductivity measurements for electrolyte solutions were conducted at various temperatures in a calibrated two-electrode cell using stainless steel 316L wires, which was prepared and sealed in Ar before testing. Measurements were made by a Bio-Logic SP-200 impedance analyzer using a 10 mV ac amplitude signal and sweeping from 200 kHz to 10 Hz, using the real impedance at the point of lowest phase angle as the solution impedance. Thermal measurements were made *via* a type-K thermocouple attached to the cell wall, which was used to verify the thermal equilibrium prior to the conductivity measurement.

Results

Electrochemical characterization

The electrochemical performances of a Si composite anode for LIBs were evaluated with three electrolyte solutions ($LiPF_6$/EC/DEC, $LiPF_6$/EC/DEC/FEC, and LiFSI/EMIFSI). Fig. 1(a) shows the typical initial charge and discharge voltage profiles of the Si

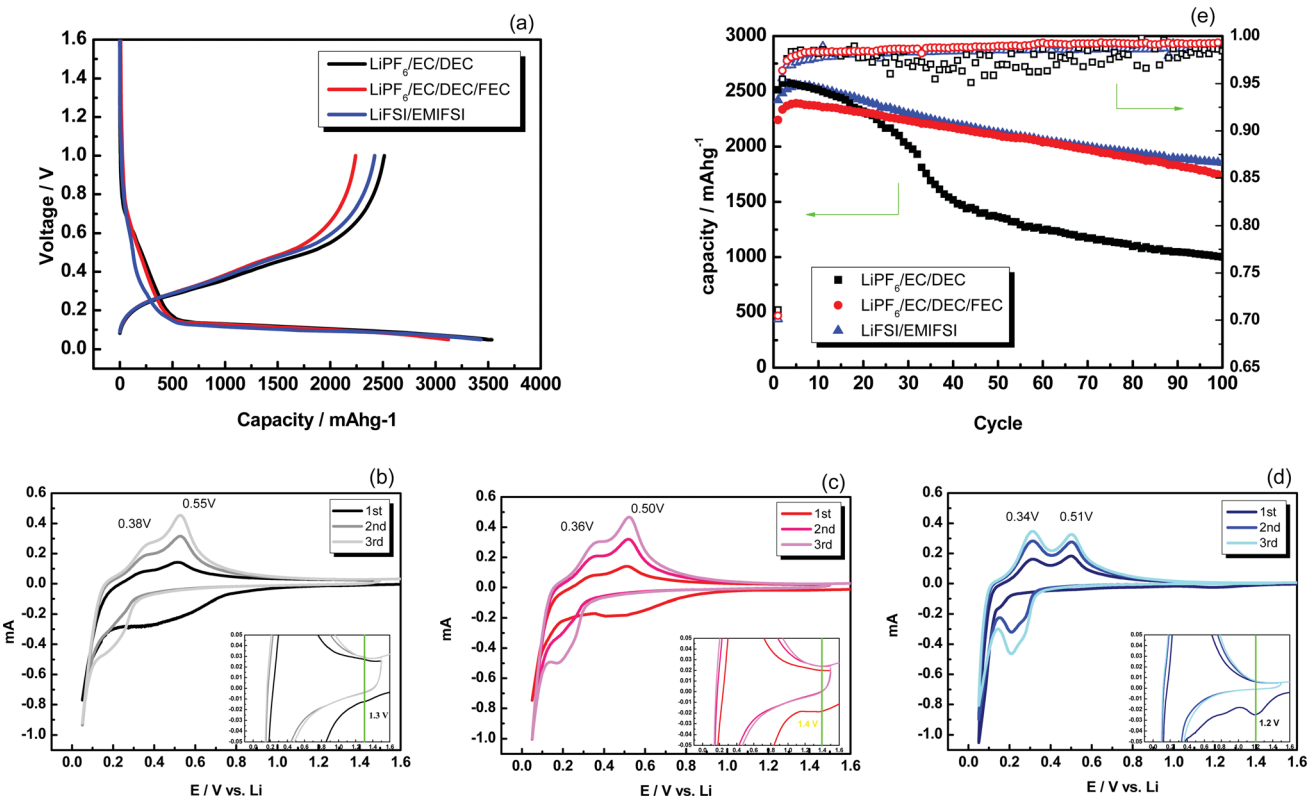

Fig. 1 (a) First charge and discharge profiles of Si anode for $LiPF_6$/EC/DEC, $LiPF_6$/EC/DEC/FEC and LiFSI/EMIFSI electrolyte. CV of Si anode in the first three cycles for (b) $LiPF_6$/EC/DEC, (c) $LiPF_6$/EC/DEC/FEC, and (d) LiFSI/EMIFSI electrolyte. (e) Cycling performance of capacity retention (closed symbols) and coulombic efficiency (open symbols) for 100 cycles of the Si anode with $LiPF_6$/EC/DEC, LiPF6/EC/DEC/FEC and LiFSI/EMIFSI.

Published on 30 August 2016. Downloaded by University of California - San Diego on 10/15/2019 6:23:28 PM.

anode with the three electrolytes within the potential window of 0.05–1.0 V. The ratio of the charge and discharge capacity describes the C.E. In the first cycle, the discharge capacities are 2513, 2241, and 2422 mA h g^{-1} and the C.E.s are 71.0%, 70.1%, and 70.5% for the $LiPF_6$/EC/DEC, $LiPF_6$/EC/DEC/FEC, and LiFSI/EMIFSI electrolytes, respectively. Among the three electrolytes, the C.E.s of $LiPF_6$/EC/DEC/FEC and LiFSI/EMIFSI are slightly lower than that of $LiPF_6$/EC/DEC. The irreversible capacity is known to originate from the decomposition of the electrolyte and the formation of the SEI on the surface of the Si anode. To understand the electrochemical reaction in detail, CV studies were conducted. Fig. 1(b–d) shows the CVs of the Si anodes in each electrolyte measured over the potential window of 1.5–0.05 V at the scan rate of 1 mV s^{-1}. The initial cathodic scan of the $LiPF_6$/EC/DEC electrolyte shows a higher current indicative of SEI formation from electrolyte decomposition. Electrolyte decomposition of EC and DEC from 0.8 V to 0.2 V can be attributed to the SEI formation on the surface of the Si anode as shown in Fig. 1(b). An additional cathodic current is seen from 0.08 V until the lowest potential of 0.05 V. This is because Li_xSi compounds are formed during charge by the alloying of Li with crystalline Si. On the reverse potential sweep, two clear peaks at 0.38 V and 0.55 V in the first anodic scan can be assigned to lithium extraction processes from the Li_xSi alloy during discharge.[33,34]

When the CV curve of $LiPF_6$/EC/DEC/FEC is compared to that of $LiPF_6$/EC/DEC, an additional reductive peak is observed at 1.4 V due to the decomposition of FEC, which is not apparent after the first cycle (Fig. 1(c)). FEC is selectively decomposed before both EC and DEC to form the SEI. The anodic scan shows two clear peaks that are similar to those for $LiPF_6$/EC/DEC. Fig. 1(d) shows a CV of the Si anode in the IL electrolyte, LiFSI/EMIFSI. A new peak at 1.2 V corresponds to the decomposition of the LiFSI/EMIFSI to form the SEI in the first cathodic reaction. After this reaction, the main lithium insertion peak appears below 0.15 V in the first reduction, which corresponds to the formation of Li_xSi compounds. This CV observation in LiFSI/EMIFSI is similar to that in 1-((2-methoxyethoxy)methyl)-1-methylpiperidinium bis(trifluoromethylsulfonyl) imide.[35] The peak intensity corresponding to lithium insertion into Si and extraction from Si becomes stronger because the alloying of Li with Si is a gradual process in the first few cycles, and thus activation of Si occurs at each cycle in the initial stages.

The three electrodes were cycled at a rate of C/10 as shown in Fig. 1(e). Although the Si anode in $LiPF_6$/EC/DEC exhibits a higher discharge capacity at earlier cycles, the capacity retention at the 100th cycle is 39%. The C.E. for the Si anode cycled in $LiPF_6$/EC/DEC fluctuates (Fig. 1(e)). In contrast, the $LiPF_6$/EC/DEC/FEC and LiFSI/EMIFSI electrolytes show higher capacity retention. The FEC electrolyte additive helps achieve a discharge capacity of 1749 mA h g^{-1} after 100 cycles (capacity retention: 77%) which is over 700 mA h g^{-1} greater than that of the electrode cycled with $LiPF_6$/EC/DEC. The electrochemical cycling performance of these two carbonate type electrolytes is in good agreement with those reported in previous publications.[36–38] The electrode cycled with LiFSI/EMIFSI also exhibits stable capacity retention after 100 cycles, achieving a capacity of 1857 mA h g^{-1} (capacity retention: 76%) while the C.E. is slightly lower than that of $LiPF_6$/EC/DEC/FEC. This confirms that the FSI-based IL electrolyte gives a comparable result to that achieved with the FEC additive and could be considered as an alternative electrolyte. LiFSI/EMIFSI has a notable function as an electrolyte to alleviate significant capacity decay. These results clearly prove that LiFSI/EMIFSI has great applicability as an alternative electrolyte not only for typical graphite anodes,[24] but also for Si composite anodes.

Surface morphology

SEM observations were performed to investigate the surface morphologies and electrode thicknesses of the Si composite anodes in their pristine state and after 100 cycles with the varying electrolytes. There are few small cracks on the surface of the pristine Si anode as shown in Fig. 2(a). After cycling in $LiPF_6$/EC/DEC, several big cracks and various crack sizes (over 10 μm) are found in the electrode that isolate parts of the Si active material electrically (Fig. 2(b)). This could be a critical cause of the observed deterioration in capacity retention. The addition of 10 wt% FEC to the $LiPF_6$/EC/DEC electrolyte suppresses the Si anode from cracking to a certain extent, although we can clearly see that the surface becomes rougher and there are some changes in the surface morphology such as cracks (Fig. 2(c)). It appears that cracks are generated homogeneously over the entire Si anode. Meanwhile, the Si anode in LiFSI/EMIFSI does not show significant cracks and has a smooth surface (Fig. 2(d)). From these results, it can be assumed that the deterioration mechanism of the IL electrolyte is different from that of the carbonate electrolytes, which is an important reason for the larger polarization and capacity decay of the carbonate electrolytes.

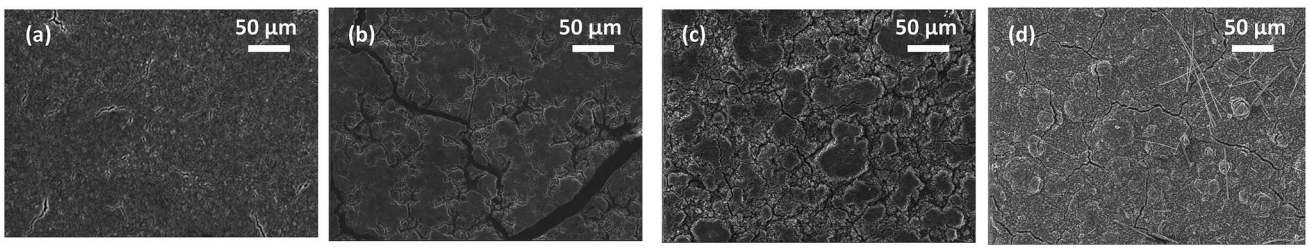

Fig. 2 SEM images of the Si anode surface (a) in its pristine state, and after 100 cycles with (b) $LiPF_6$/EC/DEC, (c) $LiPF_6$/EC/DEC/FEC and (d) LiFSI/EMI/FSI.

 This journal is © The Royal Society of Chemistry 2016

Published on 30 August 2016. Downloaded by University of California - San Diego on 10/15/2019 6:23:28 PM.

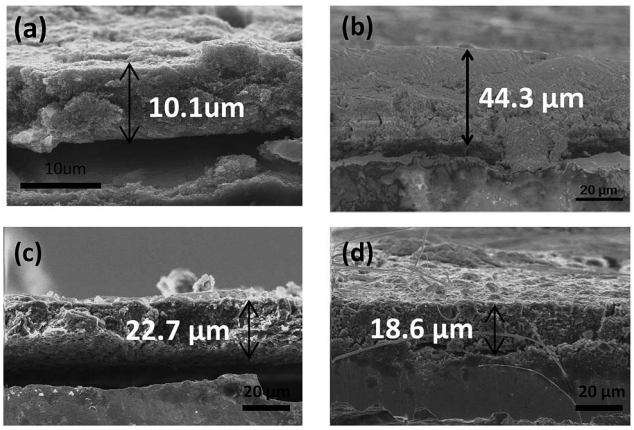

Fig. 3 Cross-sectional SEM images of the Si composite anode (a) in its pristine state, and after 100 cycles with (b) $LiPF_6$/EC/DEC, (c) $LiPF_6$/EC/DEC/FEC and (d) LiFSI/EMIFSI.

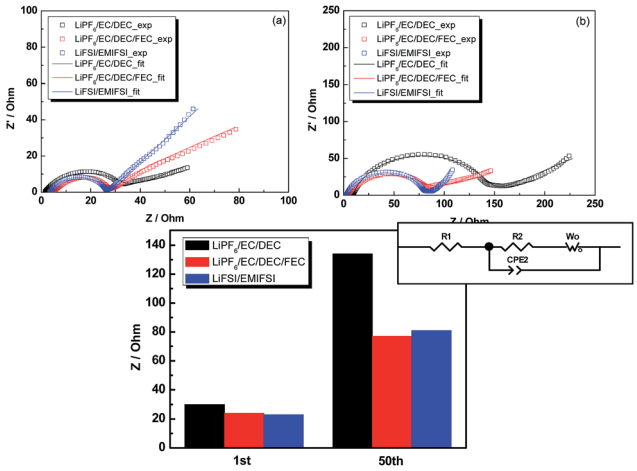

Fig. 4 EIS spectra of (a) the first and (b) the 50th cycle for $LiPF_6$/EC/DEC, $LiPF_6$/EC/DEC/FEC and LiFSI/EMI/FSI in the lithiated state. An equivalent circuit is used to model the reaction on the Si anode. The fits for the data of each anode are shown as (c) R_2 impedance between the first cycle and the 50th cycle with $LiPF_6$/EC/DEC, $LiPF_6$/EC/DEC/FEC and LiFSI/EMIFSI.

In addition to the observations of surface morphology of the Si anodes, the expansion of the anodes after 100 cycles was investigated (Fig. 3). All of the cycled electrodes were compared to the pristine electrode (uncycled), which has a total thickness of 10.1 μm (Fig. 3(a)). Fig. 3(b–d) shows that the expansion of the Si anodes in $LiPF_6$/EC/DEC, $LiPF_6$/EC/DEC/FEC and LiFSI/EMIFSI is 440%, 220% and 190%, respectively. Generally, Si particles are known to expand almost 400% during lithiation, which causes severe internal stress resulting in capacity fading.[39] After 100 cycles, the electrode cycled in $LiPF_6$/EC/DEC is the only one to expand to 440%. Although this value may not be plausible theoretically based on the volume increase of fully lithiated Si, the reason for the over expansion is the electrode's porosity and composition (50 wt% Si active material, Ketjenblack, CMC binder). Furthermore, this electrode deteriorates considerably after 100 cycles without any additives, which might be the cause of the over expansion of the Si anode. Even $LiPF_6$/EC/DEC/FEC and LiFSI/EMIFSI electrolytes cannot prevent significant expansion of the Si anode. We can confirm that the electrode cycled in $LiPF_6$/EC/DEC does not keep its original structural network, ultimately causing a poor cycling performance. The SEIs formed from cycling the electrode with $LiPF_6$/EC/DEC/FEC and LiFSI/EMIFSI also suffer from crack formation, yet maintain better electrode integrity.

Impedance spectroscopy

The interfacial behavior of the Si composite anode with the different electrolyte systems was investigated by EIS measurements. Fig. 4(a and b) shows Nyquist plots of the EIS results for the Si anodes at the first cycle and the 50th cycle in $LiPF_6$/EC/DEC, $LiPF_6$/EC/DEC/FEC, and LiFSI/EMIFSI. Each of these plots is composed of a semicircle in the medium to high frequency region and a slope in the low frequency region attributed to Warburg impedance due to the solid state lithium ion diffusion into the Si anode. The equivalent circuit parameter is shown in Fig. 4(c) fitted for R_1, the resistance of the bulk electrolyte, and the R_2–CPE_2 parallel circuit, where R_2 is the resistance of the interface between the electrodes and the electrolytes. CPE_2 describes the double-layer capacitance of the interface, and W represents Warburg impedance.

In the first cycle, R_2 values for the three electrolytes are not significantly different from one another. However, after the 50th cycle, the R_2 value of $LiPF_6$/EC/DEC is 133.7 Ω which is higher than those measured in $LiPF_6$/EC/DEC/FEC and LiFSI/EMIFSI (77.7 Ω and 80.5 Ω respectively). This is attributed to the greater pulverization of the $LiPF_6$/EC/DEC electrode which causes poor electrical conductivity as a result of the large electrode (Fig. 3). The impedance of $LiPF_6$/EC/DEC is greatly increased in comparison to those of $LiPF_6$/EC/DEC/FEC and LiFSI/EMIFSI because the $LiPF_6$/EC/DEC electrode becomes thicker than the other two electrodes (Fig. 4(d)). Many cracks formed on the surface of the Si anode cause severe degradation in electrochemical performance. The increased impedance of the $LiPF_6$/EC/DEC electrolyte is consistent with the work conducted by Mullins *et al.*[40]

Rate performance

The lower impedance and thinner electrodes may lead to the superior rate capability of $LiPF_6$/EC/DEC/FEC and LiFSI/EMIFSI. As well as the electrochemical cycle performance, the output characteristic of the battery (especially rate performance) is a considerable factor for the practical use of ILs in LIBs. The rate capability was evaluated at various rates from 0.1C to 1.0C. Fig. 5(a) illustrates the rate performance of the Si composite anode at different rates with the three electrolyte systems. All of the electrolytes show a drop in capacity when the current rates increase; however, the LiFSI/EMIFSI electrolyte shows the best rate capability. The capacity retention at 1.0C of the electrode cycled with LiFSI/EMIFSI is 78%. After the 1C rate test has been conducted and the current is lowered to 0.1C, the specific capacities of the LiFSI/EMIFSI and $LiPF_6$/EC/DEC/FEC

Published on 30 August 2016. Downloaded by University of California - San Diego on 10/15/2019 6:23:28 PM.

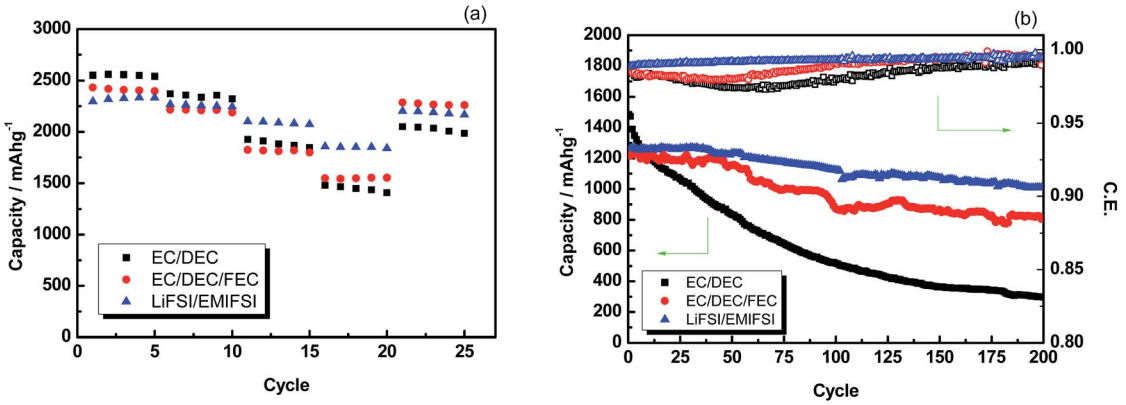

Fig. 5 (a) Rate capabilities and (b) long term 2C rate cycle performances of the Si anode with $LiPF_6$/EC/DEC, $LiPF_6$/EC/DEC/FEC and LiFSI/EMIFSI. Specific capacity (closed symbols) and C.E. (open symbols).

cycled electrodes mostly recover to their original levels. This indicates that the poor rate performance of $LiPF_6$/EC/DEC might be attributed to the cracks on the surface and the thicker electrode due to the severe decomposition of the electrode after cycling.

To elucidate the differences of electrode performance obtained in $LiPF_6$/EC/DEC/FEC and LiFSI/EMIFSI, the electrodes were cycled 200 times at 2C. Fig. 5(b) shows a rate performance comparison of the three electrolyte systems at the 2C rate. LiFSI/EMIFSI exhibits a better rate capability and higher C.E. even at high current compared to $LiPF_6$/EC/DEC and $LiPF_6$/EC/DEC/FEC. At the end of the 200th cycle, the Si anode in LiFSI/EMIFSI shows better capacity retention based on the highest remaining specific capacity among the Si anodes. These results suggest that LiFSI/EMIFSI is an effective electrolyte for Si composite anodes to improve battery performance. Generally, FEC is a well-known additive that enhances the electrochemical performance of Si composite anodes, however, in terms of rate performance LiFSI/EMIFSI outperforms $LiPF_6$/EC/DEC/FEC.

In order to further investigate this phenomenon, the ionic conductivity of each electrolyte was examined over a broad temperature range (Fig. 2S, ESI†). This is of particular importance because the ionic conductivity affects the function of the active material and battery performance. The ionic conductivities of $LiPF_6$/EC/DEC and $LiPF_6$/EC/DEC/FEC are almost the same at each temperature and the ionic conductivity of LiFSI/EMIFSI is lower than those of the carbonate-based electrolytes. The values for $LiPF_6$/EC/DEC and $LiPF_6$/EC/DEC/FEC at 20 °C are 7.1 mS cm^{-1} and 7.3 mS cm^{-1}, respectively, whereas the value of LiFSI/EMIFSI is 6.4 mS cm^{-1} at 20 °C. As explained above, LiFSI/EMIFSI displays higher retention than the carbonate-based electrolytes even though it has an overall lower ionic conductivity. Although measurements of the lithium transference number were not made in this study, it is assumed that there are differences in the SEI formation or stability in the electrode-electrolyte interface which improve the high-rate performance.

The electrode morphology and EIS behavior of $LiPF_6$/EC/DEC/FEC and LiFSI/EMIFSI are almost the same, thus it is difficult to explain the difference in the rate performance between the two electrolytes. There may be a mechanism which enables the Si anode of LiFSI/EMIFSI to enhance the rate performance to a greater extent than is found in carbonate type electrolytes; therefore, the chemical composition and evolution of the SEI need to be investigated.

Surface analysis of the cycled Si composite anode by XPS

To understand the superior rate capability of the IL electrolyte, the chemical composition of the SEI was analyzed. XPS analysis was conducted in the lithiated state after 100 cycles. Before the Si anodes were analyzed, the electrodes were washed thoroughly with acetonitrile to make sure that there was no remaining Li salt or solvent residue on the electrodes. Detailed scans of all prepared Si anodes were collected from the C 1s, O 1s, Li 1s, and F 1s spectra.

The O 1s spectra of the Si anode after 100 cycles are shown in Fig. 6(a). Several oxygenated compounds are convoluted as broad peaks in both $LiPF_6$/EC/DEC and $LiPF_6$/EC/DEC/FEC. These are attributed to carbonate, carbonyl, ether, other carbonate species ($ROCOO^-$), and PO_xF_y species. This result is consistent with data from the experiment conducted by Edström *et al.*[37] The O 1s spectra of the $LiPF_6$/EC/DEC and $LiPF_6$/EC/DEC/FEC electrolytes correspond well to the species found in the C 1s spectra (Fig. 3Sa, ESI†). The composition of the SEI is primarily carbonates with lower amounts of ether, alkoxide, alkyls, and alkenes. Both electrolytes yield LiF after 100 cycles (Fig. 3Sb, ESI†).

On the other hand, the XPS spectra of the Si anode cycled in LiFSI/EMIFSI show a very different surface structure and chemical composition. For the O 1s spectra of LiFSI/EMIFSI, peaks are identified as Li_2O at 528 eV, SO_2^{2-} at 530 eV, and LiOH at 531 eV.[41,42] As shown in Fig. 6(b), LiOH is present at a higher composition percentage compared to Li_2O and SO_2^{2-} functionalities. The presence of O and S containing species are the result of the decomposition of the FSI anion to form the SEI on the Si anode. The decomposition species of the EMI cation also contributes to the SEI, as indicated by the CN components shown in Fig. 3Sa (ESI†).[43]

 This journal is © The Royal Society of Chemistry 2016

Published on 30 August 2016. Downloaded by University of California - San Diego on 10/15/2019 6:23:28 PM.

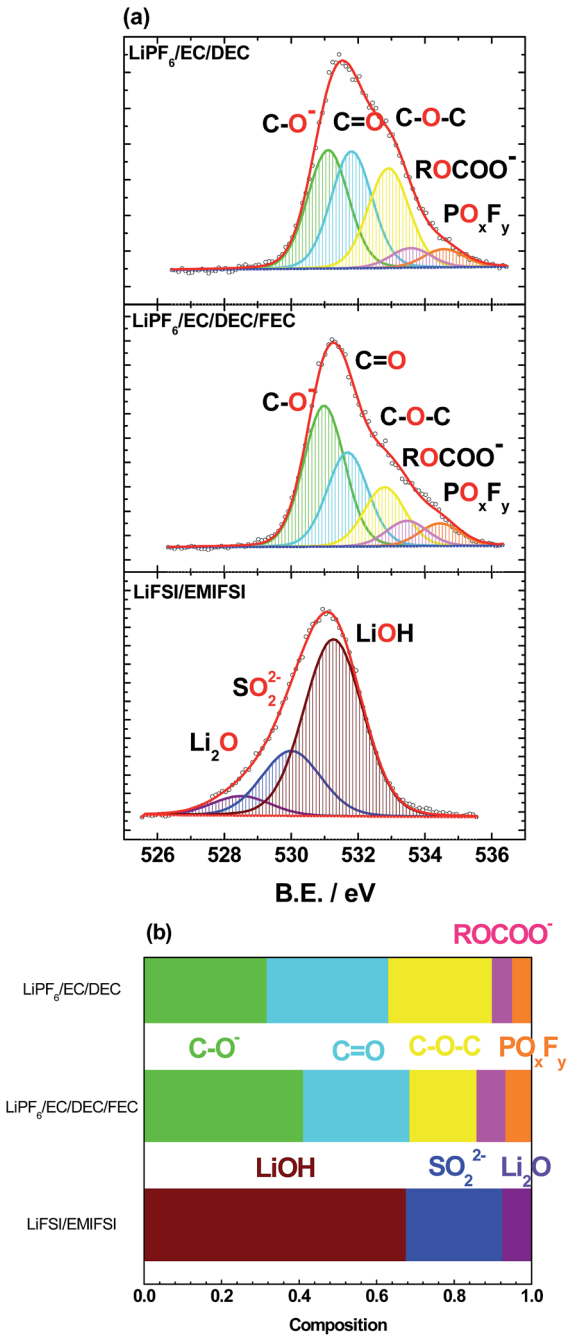

Fig. 6 (a) O 1s spectra of the Si composite anode after 100 cycles with $LiPF_6$/EC/DEC, $LiPF_6$/EC/DEC/FEC and LiFSI/EMIFSI. (b) Relative composition of the SEIs based on the O 1s spectra.

Discussion

On the basis of the above results concerning the electrochemical performances, electrode morphology, and SEI formation of the three electrolytes, the mechanism of the improved electrochemical performance of the electrode cycled in LiFSI/EMIFSI is discussed here. The ionic conductivity of LiFSI/EMIFSI is slightly lower than that of the carbonate type electrolytes and the irreversible capacity at the first cycle of LiFSI/EMIFSI, which affects the total battery performance, is still larger than that of the carbonate type electrolytes. To apply this IL electrolyte in a practical battery, it would be necessary to create a more effective SEI by electrolyte modification or the use of additives. Nevertheless, LiFSI/EMIFSI outperforms $LiPF_6$/EC/DEC/FEC electrochemically. The initial cathodic electrochemical behavior of LiFSI/EMIFSI is similar to that of $LiPF_6$/EC/DEC/FEC, and shows a new peak at 1.2 V (Fig. 1(d)). That polarization peak is assigned to the decomposition of the EMI cation and FSI anion to form the SEI on the Si anode. Compared to the carbonate electrolytes, the surface morphology of the Si anode in LiFSI/EMIFSI shows less cracking and electrical isolation which prevent consecutive reactions with the electrolyte. As a result, the SEI formed from LiFSI/EMIFSI is thought to preserve the contact between the Si particles, carbon particles, and CMC binder. This prevents the Si anode from suffering increasing electrochemical impedance, and maintains the ionic pathway inside the electrode during repeated charging and discharging.

The Si composite anode cycled in the LiFSI/EMIFSI electrolyte has the highest performance, especially rate performance, among the three electrolyte systems in this study. The depletion of the electrolyte may sometimes occur upon electrochemical cycling affecting the cells performance; however, in this study it is confirmed by disassembling the coin cells that after prolonged electrochemical cycling, both the electrode and separator remained moist. The decomposition mechanism of LiFSI/EMIFSI on the Si composite anode is not well understood. To understand the mechanism in detail, we need to investigate the surface chemistry at different states of charge (SOC) with XPS. Moreover, it would be more effective to use TOF-SIMS for a better understanding of how the SEI forms and how thick it is on the surface; we will pursue this in future research. However, the results of the current study may be used to explain the electrochemical performance systematically. The electrode thicknesses of Si after cycling in $LiPF_6$/EC/DEC/FEC and LiFSI/EMIFSI are comparable while the electrode thickness of Si cycled in $LiPF_6$/EC/DEC is substantially thicker. The thinner electrodes help to improve the electrochemical performance, which is evident from the higher capacity retention over cycling at C/10, and the lower impedance. While the low rate performance may be similar for the two electrolytes, the performance of LiFSI/EMIFSI at higher rates is greater than that of the $LiPF_6$/EC/DEC/FEC electrolyte (Fig. 5(b)). This improved rate performance may be understood by the substantially different SEI components found using each electrolyte. LiFSI/EMIFSI decomposes prior to the decomposition of EC or DEC to form an initial SEI, which consists of larger amounts of inorganic species such as LiOH, Li_2O, SO_2^{2-} and LiF. Some studies have shown that a high amount of LiF rather than organic species is correlated to an improvement of electrochemical performance.[44,45] The function of the SO_2^{2-} is not yet clear, but one hypothesis is that SO_2^{2-} might contribute to the maintenance of a stable SEI and so influence the electrochemical performance.[46] Harris *et al.* investigated the effects of the SEI species using XPS analysis and EIS, stating that organic species are highly resistive. Conversely, inorganic species generally have more ion conductive properties resulting in lower impedance.[47]

Published on 30 August 2016. Downloaded by University of California - San Diego on 10/15/2019 6:23:28 PM.

In addition, having LiOH may be considered to lead to preferred lithium ion diffusion through the SEI, which may have the effect of enhancing the rate capability of the Si composite anode.[48] Edstrom *et al.* found that Li_2O formed in the first, 50th and 100th cycles when the Si electrode was cycled with LiFSI/EC/DEC.[31] They stated that the Li_2O may be one of the components that improves the electrochemical performance. The use of LiFSI rather than $LiPF_6$ might also be a contributing factor in enhancing the electrochemical performance of the Si anode. Most studies have demonstrated the relationship between battery performance and surface chemistry by using conventional electrolytes. Replacing $LiPF_6$ with other salts may facilitate the development of a stable and high rate electrochemical performance for the Si anode.

This means that inorganic species might be considered as the preferred SEI components for lithium ion diffusion, despite the lower ionic conductivity of LiFSI/EMIFSI. Furthermore, the LiFSI electrolyte tends to have a higher lithium transference number than $LiPF_6$ in carbonate-based solvents (*ca.* 0.55 *vs.* 0.4).[49,50] This higher lithium transference number (lithium ion conductivity) may also improve the rate performance in the present study. Qian *et al.* demonstrated that even highly concentrated electrolyte using LiFSI can achieve a high rate cycle performance in spite of having lower ionic conductivity and higher viscosity.[51] This is due to the low reactivity of the electrolyte and the high lithium transference number which allow a high C.E. to be maintained throughout prolonged cycles. As shown in this study, the C.E. of LiFSI/EMIFSI showed the higher electrochemical stability of this electrolyte from the beginning to the end, whereas the carbonate electrolytes showed unstable behavior (Fig. 5(b)). This might be ascribed to the higher lithium transference number of LiFSI/EMIFSI.

It is clear that the degradation components from the LiFSI/EMIFSI-based electrolyte form a stable SEI, preventing further decomposition and maintaining electrochemical performance in the half cells. All of our results suggest that faster lithium ion diffusion and the presence of inorganic species, such as LiOH and Li_2O, in the SEI on the Si composite anode in LiFSI/EMIFSI play an important role in facilitating the electrochemical reaction. The behavior of LiFSI/EMIFSI in full cells is still to be studied and will require further investigation.

Conclusion

We have investigated the correlations between electrochemical properties, electrode morphology, and surface chemistry of a Si composite anode in $LiPF_6$/EC/DEC, $LiPF_6$/EC/DEC/FEC and LiFSI/EMIFSI electrolytes. The cycling performance and impedance of the electrode in $LiPF_6$/EC/DEC degrade significantly after cycling. The presence of FEC tends to suppress this degradation reaction. However, while the surface reaction and electrode morphology of $LiPF_6$/EC/DEC/FEC greatly improves the electrochemical performance for LIBs, the FEC content in the electrolyte eventually diminishes after cycling which leads to a performance drop. As a result, carbonate-based electrolytes may not offer a solution to issues for Si composite anodes.

The LiFSI/EMIFSI electrolyte leads to a higher electrochemical performance and lower interfacial resistance on the Si composite anode. It also exhibits superior rate capability despite its slightly lower ionic conductivity. Carbonate type electrolytes lead to an SEI with a large quantity of organic species. In contrast, the decomposed components of the LiFSI/EMIFSI making up the SEI form inorganic species such as LiOH and Li_2O as the dominant products on the Si anode. Our study suggests that the inorganic species in the SEI have the ability to promote Li ion diffusion, so improving the electrochemical reaction on the surface of the Si anode, which enhances the cycle performance. The IL used in this study is a promising electrolyte for a safer, long-life and high capacity Si anode.

Acknowledgements

The majority of this work is funded by the Assistant Secretary for Energy Efficiency and Renewable Energy, Office of Vehicle Technologies, U.S. Department of Energy under Contract No. DE-AC02-05CH11231, Subcontract No. 7073923 under the Advanced Battery Materials Research (BMR) Program. J. A. and Y. S. M. would like to thank Dr Keith J. Stevenson, Dr Hugo Celio, and Caleb Alexander for their help and thoughtful discussions regarding XPS experiments at the Texas Materials Institute at UT Austin. The SEM analysis in this work was performed in part at the San Diego Nanotechnology Infrastructure (SDNI), a member of the National Nanotechnology Coordinated Infrastructure, which is supported by the National Science Foundation (Grant ECCS-1542148). H. S. and Y. S. M. are grateful for the partial funding from Asahi Kasei Corporation.

References

1 M. Armand and J.-M. Tarascon, *Nature*, 2008, **451**, 652–657.
2 J.-M. Tarascon and M. Armand, *Nature*, 2001, **414**, 359–367.
3 Y. Wang and J. Y. Lee, *J. Phys. Chem. B*, 2004, **108**, 17832–17837.
4 Y. Liu, T. Matsumura, N. Imanishi, N. Ichikawa, A. Hirano and Y. Takeda, *Electrochem. Commun.*, 2004, **6**, 632–636.
5 S. T. Chang, I. C. Leu, C. L. Liao, J. H. Yen and M. H. Hon, *J. Mater. Chem.*, 2004, **14**, 1821–1826.
6 Y. Kim, Y. Yoon and D. Shin, *J. Anal. Appl. Pyrolysis*, 2009, **85**, 557–560.
7 J. Li and J. R. Dahn, *J. Electrochem. Soc.*, 2007, **154**, A156–A161.
8 B. Key, R. Bhattacharyya, M. Morcrette, V. Seznéc, J.-M. Tarascon and C. P. Grey, *J. Am. Chem. Soc.*, 2009, **131**, 9239–9249.
9 H. Li, X. Huang, L. Chen, Z. Wu and Y. Liang, *Electrochem. Solid-State Lett.*, 1999, **2**, 547–549.
10 J. Graetz, C. C. Ahn, R. Yazami and B. Fultz, *Electrochem. Solid-State Lett.*, 2003, **6**, A194–A197.
11 M. Green, E. Fielder, B. Scrosati and M. Wachtler, *Electrochem. Solid-State Lett.*, 2003, **6**, A75–A79.
12 X. Chen, K. Gerasopoulos, J. Guo, A. Brown, C. Wang, R. Ghodssi and J. N. Culver, *ACS Nano*, 2010, **4**, 5366–5372.

 This journal is © The Royal Society of Chemistry 2016

Published on 30 August 2016. Downloaded by University of California - San Diego on 10/15/2019 6:23:28 PM.

13 J. H. Ryu, J. W. Kim, Y.-E. Sung and S. M. Oh, *Electrochem. Solid-State Lett.*, 2004, **7**, A306–A309.
14 L. Y. Beaulieu, K. W. Eberman, R. L. Turner, L. J. Krause and J. R. Dahn, *Electrochem. Solid-State Lett.*, 2001, **4**, A137–A140.
15 T. R. Hatchard and J. R. Dahn, *J. Electrochem. Soc.*, 2004, **151**, A838–A842.
16 B. PhiLiPpe, R. Dedryvère, J. Allouche, F. Lindgren, M. Gorgoi, H. Rensmo, D. Gonbeau and K. Edström, *Chem. Mater.*, 2012, **24**, 1107–1115.
17 P. Verma, P. Maire and P. Novák, *Electrochim. Acta*, 2010, **55**, 6332–6341.
18 Z. Zhang, M. Zhang, Y. Wang, Q. Tan, X. Lv, Z. Zhong, H. Li and S. Fabing, *Nanoscale*, 2013, **5**, 5384–5389.
19 R. McMillan, H. Slegr, Z. X. Shu and W. Wang, *J. Power Sources*, 1999, **81–82**, 20–26.
20 K. Schroder, J. Alvarado, T. A. Yersak, J. Li, N. Dudney, L. J. Webb, Y. S. Meng and K. J. Stevenson, *Chem. Mater.*, 2015, **27**, 5531–5542.
21 A. Noda, K. Hayamizu and M. Watanabe, *J. Phys. Chem. B*, 2001, **105**, 4603–4610.
22 Z.-B. Zhou, H. Matsumoto and K. Tatsumi, *Cyclic Quaternary Ammonium Ionic Liquids with Perfluoroalkyltrifluoroborates: Synthesis, Characterization, and Properties*, Wiley, 2006, vol. 12, pp. 2196–2212.
23 K. Kumai, H. Miyashiro, Y. Kobayashi, K. Takei and R. Ishikawa, *J. Power Sources*, 1999, **81–82**, 715–719.
24 Y. Matsui, M. Yamagata, S. Murakami, Y. Saito, T. Higashizaki, E. Ishiko, M. Kono and M. Ishikawa, *J. Power Sources*, 2015, **279**, 766–773.
25 D. M. Piper, T. Evans, K. Leung, T. Watkins, J. Olson, S. C. Kim, S. S. Han, V. Bhat, K. H. Oh, D. A. Buttry and S.-H. Lee, *Nat. Commun.*, 2015, **6**, 6230.
26 K. M. Schroder, H. Celio, L. J. Webb and K. J. Stevenson, *J. Phys. Chem. C*, 2012, **116**, 19737–19747.
27 K. W. Schroder, A. G. Dylla, S. J. Harris, L. J. Webb and K. J. Stevenson, *ACS Appl. Mater. Interfaces*, 2014, **6**, 21510–21524.
28 G. Beamson and D. Briggs, *High Resolution XPS of Organic Polymers, The Scienta ESCA 300 Database*, John Wiley & Sons, 1992.
29 T. Y. Leung, W. F. Man, P. K. Lim, W. C. Chan, F. Gaspari and S. Zukotynski, *J. Non-Cryst. Solids*, 1999, **254**, 156–160.
30 K. Edström, T. Gustafsson and J. O. Thomas, *Electrochim. Acta*, 2004, **50**, 397–403.
31 B. PhiLiPpe, R. Dedryvère, M. Gorgoi, H. Rensmo, D. Gonbeau, K. Edström, R. Dedryvere and K. Edstrom, *J. Am. Chem. Soc.*, 2013, **135**, 9829–9842.
32 P. Verma, P. Maire and P. Novák, *Electrochim. Acta*, 2010, **55**, 6332–6341.
33 I. A. Profatilova, C. Stock, A. Schmitz, S. Passerini and M. Winter, *J. Power Sources*, 2013, **222**, 140–149.
34 N.-S. Choi, K. H. Yew, K. Y. Lee, M. Sung, H. Kim and S.-S. Kim, *J. Power Sources*, 2006, **161**, 1254–1259.
35 M. Shimizu, H. Usui, T. Suzumura and H. Sakaguchi, *J. Phys. Chem. C*, 2015, **119**, 2975–2982.
36 V. Etacheri, O. Haik, Y. Goffer, G. A. Roberts, I. C. Stefan, R. Fasching and D. Aurbach, *Langmuir*, 2012, **28**, 965–976.
37 C. Xu, F. Lindgren, B. PhiLiPpe, M. Gorgoi, F. Björefors, K. Edström and T. Gustafsson, *Chem. Mater.*, 2015, **27**, 2591–2599.
38 H. Nakai, T. Kubota, A. Kita and A. Kawashima, *J. Electrochem. Soc.*, 2011, **158**, A798–A801.
39 B. A. Boukamp, G. C. Lesha and R. A. Huggins, *J. Electrochem. Soc.*, 1981, **128**, 725–729.
40 Y.-M. Lin, K. C. Klavetter, P. R. Abel, N. C. Davy, J. L. Snider, A. Heller and C. B. Mullins, *Chem. Commun.*, 2012, **48**, 7268–7270.
41 A. Budi, A. Basile, G. Opletal, A. F. Hollenkamp, A. S. Best, R. J. Rees, A. I. Bhatt, A. P. O'Mullane and S. P. Russo, *J. Phys. Chem. C*, 2012, **116**, 19789–19797.
42 C. Liu, X. Ma, F. Xu, L. Zheng, H. Zhang, W. Feng, X. Huang, M. Armand, J. Nie, H. Chen and Z. Zhou, *Electrochim. Acta*, 2014, **149**, 370–385.
43 M. Olschewski, R. Gustus, M. Marschewski, O. Höfft and F. Endres, *Phys. Chem. Chem. Phys.*, 2014, **16**, 25969–25977.
44 H. Park, S. Choi, S. Lee, G. Hwang, N.-S. Choi and S. Park, *J. Mater. Chem. A*, 2015, **3**, 1325–1332.
45 M.-H. Ryou, G.-B. Han, Y. M. Lee, J.-N. Lee, D. J. Lee, Y. O. Yoon and J.-K. Park, *Electrochim. Acta*, 2010, **55**, 2073–2077.
46 S. Xiong, K. Xie, E. Blomberg, P. Jacobsson and A. Matic, *J. Power Sources*, 2014, **252**, 150–155.
47 P. Lu, C. Li, E. W. Schneider and S. J. Harris, *J. Phys. Chem. C*, 2014, **118**, 896–903.
48 K. Tasaki, A. Goldberg, J.-J. Lian, M. Walker, A. Timmons and S. J. Harris, *J. Electrochem. Soc.*, 2009, **156**, A1019–A1027.
49 L. Li, S. Zhou, H. Han, H. Li, J. Nie, M. Armand, Z. Zhou and X. Huang, *J. Electrochem. Soc.*, 2011, **158**, A74–A82.
50 K. Hayamizu, *J. Chem. Eng. Data*, 2012, **57**, 2012–2017.
51 J. Qian, W. A. Henderson, W. Xu, P. Bhattacharya, M. Engelhard, O. Borodin and J.-G. Zhang, *Nat. Commun.*, 2015, **20**, 6362.